Structure Stability of Georgian Natural Heulandite

Vladimer Tsitsishvili[1,2*)], Nanuli Dolaberidze[3)], Nato Mirdzveli[4*)], Manana Nijaradze[5)], Zurab Amiridze[6)], Bela Khutsishvili[7)]

[1*)] Georgian National Academy of Sciences, 52, Rustaveli Ave., 0108, Tbilisi, Georgia; email: vladimer.tsitsishvili@tsu.ge; https://orcid.org/0000-0003-2592-0973

[2*)] Petre Melikishvili Institute of Physical and Organic Chemistry, I.Javakhishvili Tbilisi State University, 31 A.Politkovskaia Str., 1086 Tbilisi, Georgia; email: vladimer.tsitsishvili@tsu.ge; https://orcid.org/0000-0003-2592-0973

[3)] Petre Melikishvili Institute of Physical and Organic Chemistry, I.Javakhishvili Tbilisi State University, 31 A.Politkovskaia Str., 1086 Tbilisi, Georgia; email: nanuli.dolaberidze@tsu.ge; https://orcid.org/0000-0001-6479-2156

[4)] Petre Melikishvili Institute of Physical and Organic Chemistry, I.Javakhishvili Tbilisi State University, 31 A.Politkovskaia Str., 1086 Tbilisi, Georgia; email: nato.mirdzveli@tsu.ge; https://orcid.org/0000-0002-1755-5024

[5)] Petre Melikishvili Institute of Physical and Organic Chemistry, I.Javakhishvili Tbilisi State University, 31 A.Politkovskaia Str., 1086 Tbilisi, Georgia; email: manana.nijaradze@tsu.ge; https://orcid.org/0000-0003-0882-500X

[6)] Petre Melikishvili Institute of Physical and Organic Chemistry, I.Javakhishvili Tbilisi State University, 31 A.Politkovskaia Str., 1086 Tbilisi, Georgia; email: zurab.amiridze@tsu.ge; https://orcid.org/0000-0002-6875-2773

[7)] Petre Melikishvili Institute of Physical and Organic Chemistry, I.Javakhishvili Tbilisi State University, 31 A.Politkovskaia Str., 1086 Tbilisi, Georgia; email: bela.khutsishvili@tsu.ge; https://orcid.org/0000-0003-3685-9506

http://doi.org/10.29227/IM-2024-01-56

Submission date: *15.2.2023* | Review date: *10.3.2023*

Abstract

Zeolites have a unique set of molecular-sieve, sorption, ion exchange and catalytic properties due to their framework microporous structure, and structural stability is an important characteristic and often a decisive factor in the application and performance of natural zeolites. The aim of our work was to study the processes occurring under the influence of heat, which determine the thermal stability of the zeolite-containing tuff of the Tedzami-Dzegvi deposit, with zeolite phase content up to 90%, consisting of heulandite and chabazite in a ratio of 8:1, and chemical composition $|Na_{0.25}K_{0.06}Ca_{0.19}Mg_{0.15}|[AlSi_{3.6}O_{9.2}]\cdot 3H_2O$. *It was found that as a result of exposure to heat, a slight dealumination of the surface of the calcined (400-500 °C) samples occurs, as well as dehydration and amorphization of the crystal structure are observed. Sample dehydration occurs in several stages: (i) most of the water (≈60% of the total water content) is continuously lost at temperatures below ≈250 °C, (ii) the part of the remainder (≈24%) is slowly dehydrated up to 650 °C, (iii) complete dehydration of the sample is achieved at ≈800 °C. Amorphization of the heulandite phase begins at temperatures above 200 °C, the transition to the metastable heulandite B phase at ≈340 °C is not fixed, but at high temperatures wairakite or another mineral of the 9.GB.05 group and quartz are formed; the chabazite phase is stable up to ≈1000 °C, and at temperatures above 1100 °C, leucite* $(K,Na)AlSi_2O_6$ *and cristobalite* SiO_2 *are formed. The adsorption of water vapor and benzene on heat-treated samples decreases monotonically with an increase in the calcination temperature, following amorphization. Nitrogen adsorption-desorption isotherms show slight decrease of the absorbent surface area with an increase in the calcination temperature and nonmonotonic changes in average mesopore diameters. It is also shown that heat treatment improves the acid resistance of heulandite by reducing dealumination after sample treatment with hydrochloric acid.*

Keywords: structure stability, thermal stability, natural heulandite, georgia

Introduction

Zeolites, aluminosilicates of the general formula $M_x[Al_xSi_yO_{2(x+y)}]\cdot mH_2O$ ($M^+ = Na^+, K^+, \ldots ½Ca^{2+}, ½Mg^{2+}, \ldots$), have a unique set of molecular-sieve, sorption, ion exchange and catalytic properties due to their framework microporous structure, and structural stability is an important characteristic and often a decisive factor in the application and performance of natural zeolites. The most important factor determining the balance of the three components of the zeolite crystal structure (negatively charged framework $[AlSi_nO_{2(1+n)}]^-$, cations M^+ and water molecules) is temperature. The resistance of a zeolite structure to heat is primarily determined by the content of aluminum atoms in the framework [1], and ultra-stable synthetic zeolites with a high Si/Al molar ratio have been used in catalysis for more than half a century [2]. The cationic content also affects the thermal properties of zeolites: potassium ions K^+ may thermodynamically stabilize a certain zeolitic frameworks [3]. Preliminary heat treatment can be used to improve the properties of natural zeolites [4], and in this case, the stability of the zeolite framework also plays an important role. On the other hand, acid treatment is also used to modify zeolites, and pre-heat treatment may affect the acid resistance of the sample.

When the zeolite is heated, water is released from its structure, and such dehydration is accompanied by phase transitions and other processes that establish equilibrium under new conditions. A powerful tool for studying the stability of the structure of zeolites is thermogravimetric analysis, first applied in the early 1950s, when zeolites were divided into four types depending on the nature of the dehydration process [5]. Later it was found that in in clinoptilolite (HEU type zeolite with Si/Al>4) there are no transitions or

reactions up to approximately 750 °C, while heulandite (HEU type zeolite with Si/Al>4) is far from being so stable [6]; a detailed description of dehydration and phase transitions in heulandite was published in the mid-1980s [7].

The aim of our work was to study the processes occurring under the influence of heat, which determine the thermal stability of the zeolite-containing tuff of the Tedzami-Dzegvi deposit, Eastern Georgia, selected for thermal and acid-base modification to create new bactericidal zeolite filter materials for purification and disinfection of water from various sources.

Materials and Methods

Samples of heulandite-clinoptilolite-containing tuff were collected in the southern section of the Tedzami-Dzegvi deposit, Eastern Georgia. According to the data of chemical analysis and the powder X-ray diffraction pattern [8], they contain up to ≈90% of zeolite phase with empirical formula of dehydrated sample $(Na_{1.96}K_{0.47}Ca_{1.49}Mg_{1.17})[Al_{7.8}Si_{28.2}O_{72}]$, and are high-silica heulandites mixed with a small amount (≈10%) of chabazite (crystal chemical data $|Ca_6(H_2O)_{40}|[Al_{12}Si_{24}O_{72}]$-**CHA** [9, pp. 96-97]). Zeolitic tuff was crushed on a standard crusher, fractionated to a particle size of 1-1.4 mm or 14-16 mesh, washed with distilled water or dilute HCl solution (0.025 N) to remove clay impurities, and dried at a temperature of 95-100 °C.

Calcination of prepared samples in the temperature range of 200-800 °C was carried out in muffle furnace B400/410 (Naberthem, Carl Stuart Group), the maximum calcination temperature (800 °C) was chosen in accordance with reported thermal stability of the main impurity, CHA type zeolite [10, p. 58]; additional annealing was carried out in the temperature range of 900-1100 °C. Zeolite samples with a particle size of 1.0-1.4 mm were placed in a muffle furnace in heat-resistant round-bottom cups in the amount of 100 g, subjected to heat treatment under static conditions for 1 hour, and then, after a while, these cups was placed in desiccators with calcined $CaCl_2$ until complete cooling of the heat-treated zeolite samples. Acid treatment of samples was carried out in a shaking water bath (OLS26 Aqua Pro, Grant Instruments, US) with HCl solutions (0.5, 1.0 and 2.0 N) at a solid/liquid ratio of 1:10 in three stages (3 – 2 – 1 hour) at 75 °C.

Thermogravimetric analysis was based on weight loss (TG), difference thermal analysis (DTA) and difference thermogravimetric (DTG) curves recorded on an NETZSCH STA 2500 Regulus thermal analyzer at a heating rate of 10 °C/min. Chemical composition of samples was calculated from the X-ray energy dispersive (XRED) spectra obtained from scanning electron microscope JSM-6490LV (Jeol, Japan) equipped with INCA Energy 350 XRED analyzer (Oxford, UK). Powder X-ray diffraction (XRD) patterns were obtained from D8 Endeavor diffractometer (Bruker, Germany) employing the Cu-K_α line (λ = 0.154056 nm); the samples were scanned in the 2Θ range of 5° to 100° with a 0.02° step at a scanning speed of 1°/min. The adsorption capacity for water and benzene vapors was measured under static conditions at room temperature. Nitrogen adsorption/desorption isotherms were measured at 77 K using ASAP 2020 Plus analyzer (Micromeritics, USA) using Brunauer–Emmett–Teller (BET) and Barrett-Joyner-Halenda (BJH) models for data analysis.

Results and Discussion

The results of thermogravimetric analysis of the original sample, as well as the chemical composition, powder XRD patterns and adsorption characteristics of the heat-treated samples, are considered.

Thermal analysis

Thermogravimetric curves of Georgian heulandite are presented in Fig. 1. The measured total weight loss (15.09%) is in good agreement with the calculated (15.5%) based on the empirical chemical formula $(Na_{0.25}K_{0.06}Ca_{0.19}Mg_{0.15})$ $[AlSi_{3.6}O_{9.2}]$) of dehydrated zeolite and the assumption that there are 3 water molecules per aluminum atom, as follows from the heulandite crystal chemical data $|Ca_4(H_2O)_{24}|$ **[**$Al_8Si_{28}O_{72}$**]-HEU** [9, pp. 156-157]. Most of the water (≈9% of the total weight and ≈60% of the total water content) is continuously lost at temperatures below ≈250 °C, and then part of the remainder (≈24% of the total content) is slowly dehydrated up to 650 °C, complete dehydration of the sample is achieved at ≈800 °C.

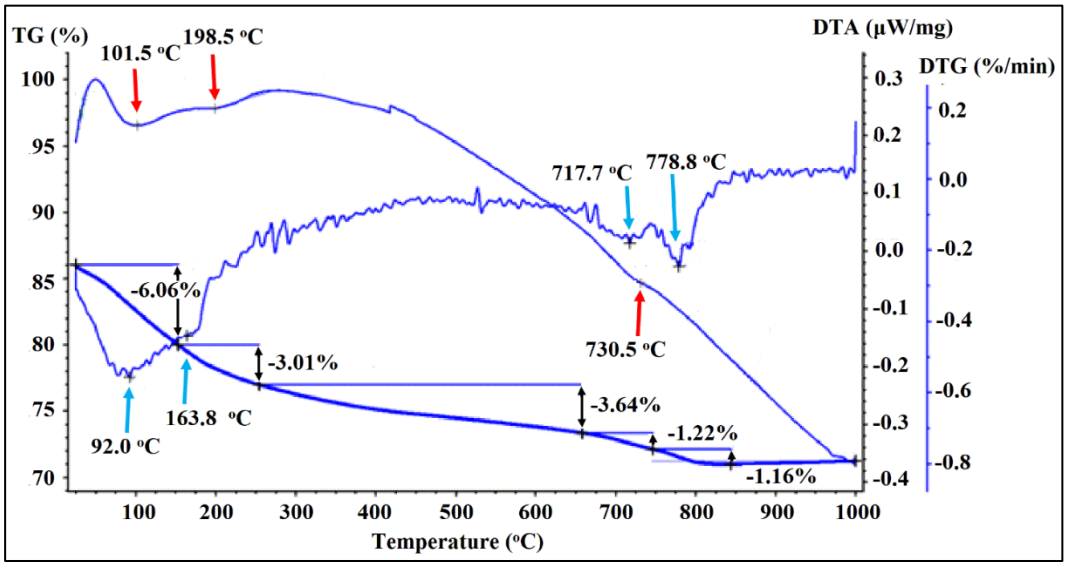

FIG. 1. Thermogravimetric curves of Georgian heulandite (red and blue arrows show endothermic peaks on DTA and DTG curve, respectively).

The DTA and DTG curves show slow endothermic changes between room temperature and 250 °C, but do not have a sharp endothermic peak at ≈340 °C, which is considered a hallmark of heulandite [10, pp. 26, 47-48, Fig. 1.14] and which is associated with the transition to the structure of "sluggish" [6] heulandite B, first described by Koizumi [5]. Probably, the absence of a

transition to heulandite B is explained by the lower aluminum content in Georgian heulandite (Si/Al=3.6) than in the samples studied in works [5-7]. It should also be noted that according to the XRED spectra, chemical composition of the surface of the calcined samples undergoes slight changes, which are most reflected in the Si/Al molar ratio (see Fig. 2) – in the temperature range of 400-500 °C, dealumination is observed; at higher temperatures, the Si/Al molar ratio almost returns to its previous values.

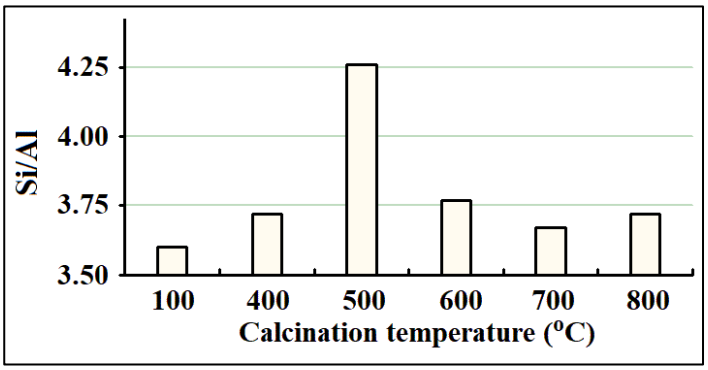

Fig. 2. The Si/Al molar ratio in calcinated samples.

High-temperature endothermic peaks indicate structural changes in the temperature range of 710-780 °C as the remaining water molecules are lost.

Powder XRD patterns

The studied zeolite is a mixture of heulandite and chabazite, the XRD pattern is a superposition, and the assignment of peaks to HEU and CHA types carried out using data from collection of simulated XRD patterns [11] and experimental pattern of synthetic chabazite from [12] is shown in Fig. 3.

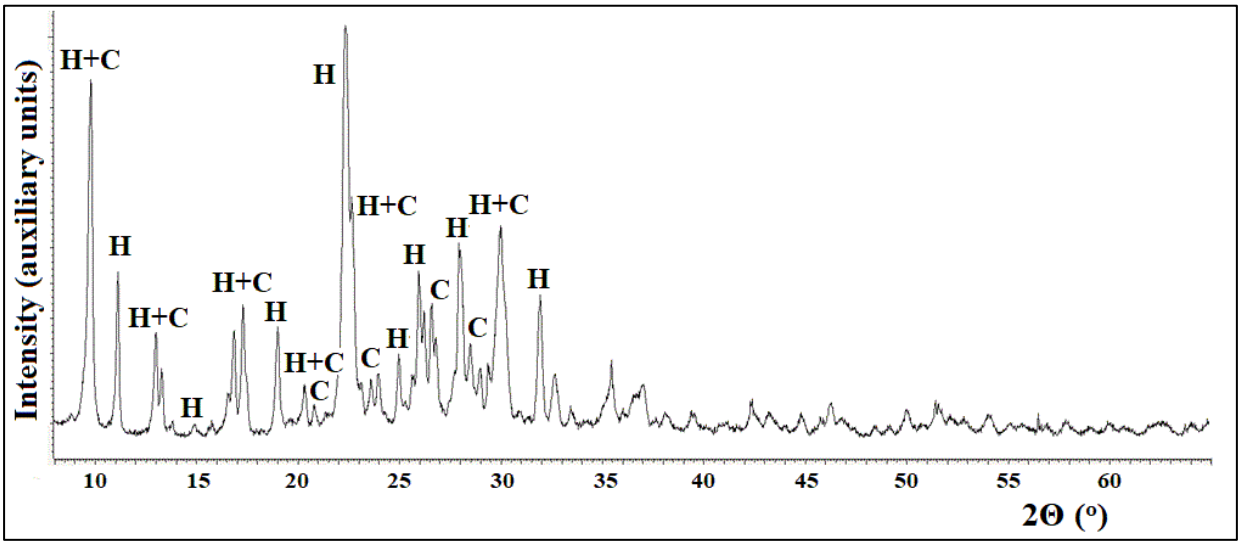

Fig. 3. Assignment of peaks in powder XRD pattern of native Georgian heulandite (H – peak of HEU, C – peak of CHA).

Powder X-ray diffraction patterns of Georgian heulandite calcined at different temperatures (Fig. 4) show following: in the temperature range up to 200 °C, the patterns do not change, at higher temperatures the peaks begin to broaden, than the intensity of the heulandite peaks decreases, a broad band and a sharp peak of quartz (2Θ = 26.6°) appear (Fig. 3b). When studying the transformations of heulandite [7], it was shown that at a temperature of 470 °C the amorphous phase begins to be formed from metastable heulandite B, and at temperatures exceeding 500 °C a mixture of quartz (SiO_2) and minerals of the 9.GB.05 group such as wairakite ($Ca(Al_2Si_4O_{12})\cdot 2H_2O$) and/or anorthite ($Ca(Al_2Si_2O_8)$) starts to appear. The most intense peaks in the XRD patterns of these minerals are observed at 2Θ ≈ 16 and 28° for wairakite and anorthite, respectively, but they can be overlapped by peaks of chabazite (reflection with *hkl*=113 giving an intense peak at 2Θ=16° [12]) and heulandite (*hkl*=-422 at 2Θ=28.1°, and *hkl*=-441 at 2Θ=28.5° [11]), and it is impossible to draw an unambiguous conclusion about the formation of these minerals.

However, the presence of high-temperature endo peaks on the TGA curve (717.7 and 778.8 °C) may indicate the "melting" of the crystal structure of these minerals. In addition, the formation of wairakite, a tectosilicate with zeolite water, explains the prolongation of the dehydration process up to high temperatures, when heulandite amorphization is already completed. At temperatures above 780 °C, all peaks of heulandite and possibly formed minerals collapse into a broad band, overlapping the sharp peaks of quartz and chabazite (Fig. 4c). The crystal structure of chabazite, a heterogeneous admixture of heulandite-bearing tuff, is preserved up to a temperature of 960 °C; at higher temperatures, the powder XRD patterns show the formation of leucite ($(K,Na)AlSi_2O_6$, two intense peaks at 2Θ = 26.0 and 27.5°) and cristobalite (SiO_2, 2Θ=22.0°).

Adsorption and porosity

Water molecules have a small kinetic diameter of 0.266 nm and can freely pass through entrance windows into heulandite channels, and the adsorption of water vapor at a relative pressure p/p_o=0.4, corresponding to almost complete filling of micropores, is a measure of their volume available for small polar molecules [13], while adsorption at saturated water vapor pressure ($p/p_o \approx 1$) is a measure of the total pore volume. The kinetic diameter of the benzene molecule (0.585 nm) significantly exceeds the sizes of micropores and channels of heulandite and chabazite, so that this non-polar molecule can be adsorbed only on the zeolite surface developed due to the presence of meso- and macropores; benzene adsorption capacity is a relative measure of surface area and its hydrophobicity.

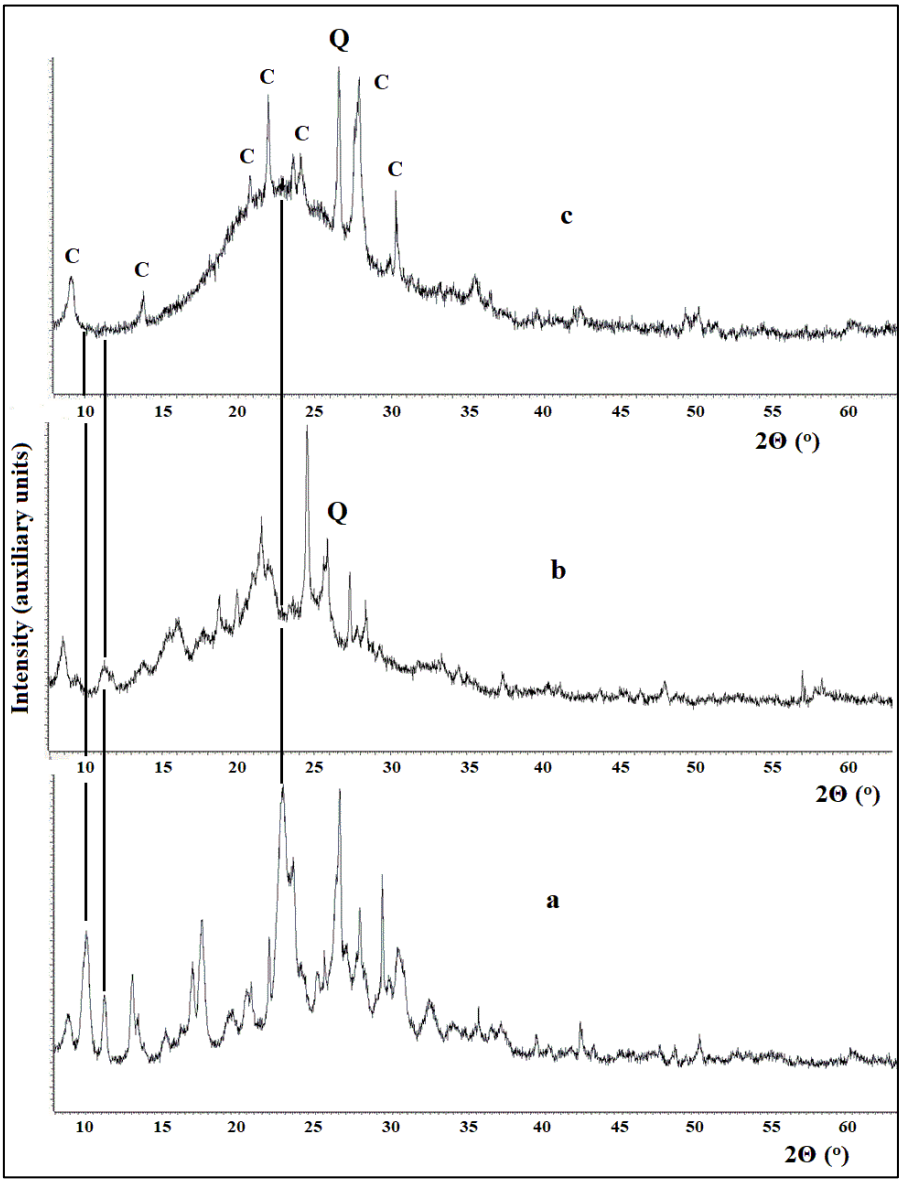

Fig. 4. Powder XRD patterns of Georgian heulandite calcined at 300 (a), 500 (b), and 800 (c) °C (C – peaks of chabazite, Q – peak of quartz, three vertical lines show position of intense heulandite peaks with *hkl*=020 at 2Θ=9.85°, *hkl*=200 at 2Θ=11.1°, and *hkl*=131 at 2Θ=22.2° [11]).

Water and benzene adsorption

According to the measurement results (Fig. 5), the adsorption capacity of micropores decreases with an increase in the calcination temperature, reaching very low values (<0.3 mmol/g) at temperatures above 500 °C, the adsorption capacity of all pores decreases monotonically with an increase in the calcination temperature; the difference between these two indicators, $a_{pores} - a_{micropores}$, proportional to the volume of mesopores, before the onset of amorphization increases from 2.66 to 3.33 mmol/g, and then decreases to 2.2 mmol/g, which indicates the effect of heat treatment on the mesopore system as well.

The adsorption of benzene molecules decreases monotonically with increasing sample calcination temperature, however, this hardly reflects a decrease in the hydrophobicity of the surface, since the adsorption of polar water molecules simultaneously decreases.

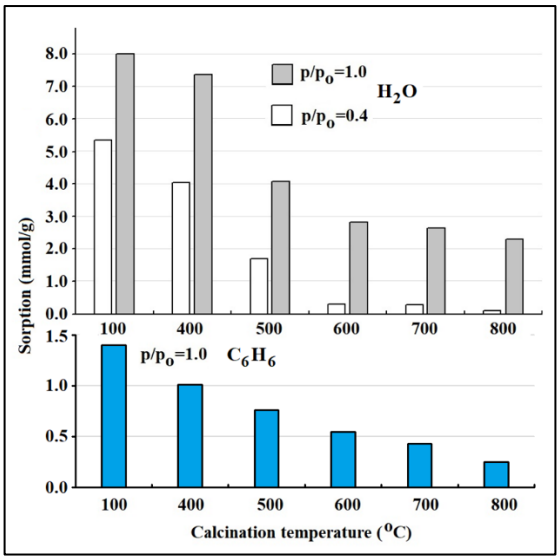

Fig. 5. Water (H_2O) and benzene (C_6H_6) sorption on Georgian heulandite calcined at different temperatures.

Nitrogen adsorption

In heulandite crystal structure, a 10-membered ring (0.75 x 0.31 nm) and one of the 8-membered rings (0.47 x 0.28 nm) cannot accommodate a nitrogen molecule (kinetic diameter 0.364 nm), which can pass only into one 8-membered ring (0.46 x 0.36 nm). The low-temperature adsorption-desorption isotherms of nitrogen on studied calcined samples correspond to the filling of micropores (Langmuir plot) at low relative pressures ($p/p_o<0.3$) and demonstrate a hysteresis loop with a jump at p/p_0= 0.4-0.5 indicating the presence of developed system of mesopores. The BET model describes the experimental data in the range of relative pressures $0.01<p/p_o<0.25$, significant discrepancies between the isotherm plot according the BET equation $(\{W[(p/p_o) - 1]\}^{-1} = (W_mC)^{-1} + \{[(C - 1)/W_mC)]\ (p/p_o)\}$, where W is adsorption at pressure p, W_m is the monolayer volume on the adsorbent surface, C is the ratio of the adsorption equilibrium constant in the first layer and the condensation constant) and the measured values occur at relative pressures $p/p_o>0.5$ (Fig. 6).

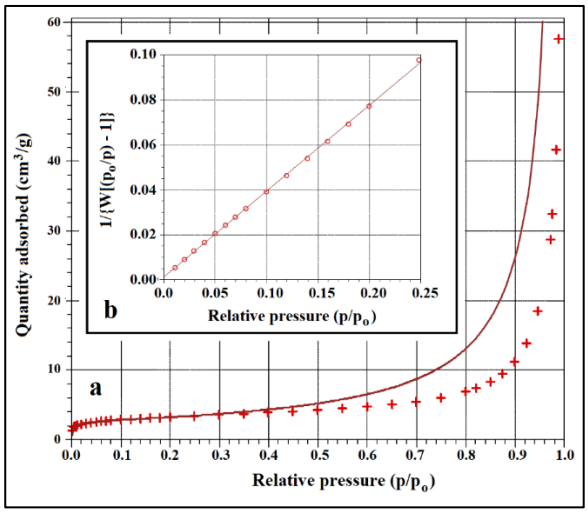

Fig. 6. Isotherm plot (**a**, solid line – calculation according to the BET equation, crosses – measured values of adsorption) and BET surface area plot (**b**).

Tab. 1. Porosity parameters according to N_2 adsorption-desorption isotherms on phillipsites.

Calcination temperature (°C)	100	400	500	600	700	800
BET surface area (m^2/g)	12.8	11.36	10.5	9.45	9.16	6.52
Total volume of pores (mm^3/g)	89.5	89.2	92.8	82.2	78.0	83.8
Volume of micropores (mm^3/g)	6.5	6.0	5.7	5.1	5.0	3.5
BET average pore diameter (nm)	28.0	31.4	35.3	34.7	34.0	51.4
BJH adsorption/desorption average pore diameter (nm)	38.0 17.2	36.3 17.6	36.2 17.6	34.3 17.2	34.0 16.1	44.5 20.1

According to the results of measurements and calculations (Table 1), the quantity of nitrogen molecules adsorbed in mesopores (at relative pressures $p/p_o>0.4$) is much greater than the quantity adsorbed in micropores ($p/p_o<0.4$), and the calculated volume of micropores available for nitrogen molecules is only 6-7% of the total pore volume, much lower than the volume of micropores available for water molecules. The BET surface area and volume of micropores decrease monotonically, the total volume of pores varies insignificantly, reaching a maximum value after calcination at 500 °C and a minimum after annealing at 700 °C. The average pore diameter calculated on the basis of the BET model increases with an increase in the calcination temperature; the application of

the BJH model gives different values from the adsorption and desorption isotherms, but the trend of changes in the pore diameter is the same. Despite the fact that the pore diameters change as a result of calcination, the nature of the pore size distribution remains the same, which is clearly seen in Fig. 7, which shows the differential pore size distribution curves dV/dD for samples calcined at different temperatures.

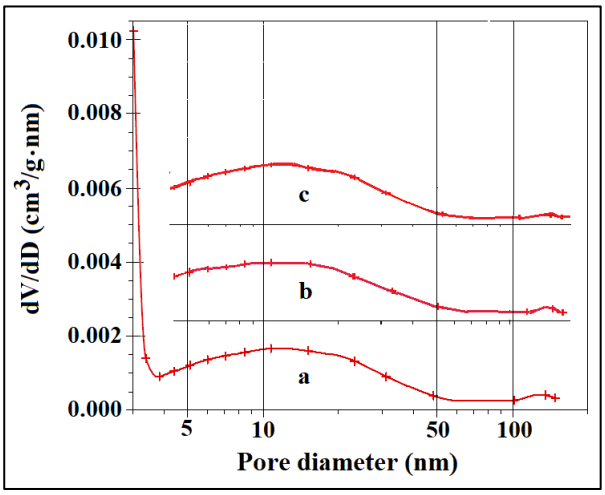

Fig. 7. Pore size distribution dV/dD curves calculated on the basis of the BJH model from desorption isotherms measured on samples calcined at 100 (a), 500 (b) and 800 (b) ºC.

Adsorption and porosity

The impact of an acidic environment on the studied zeolite leads to significant dealumination, which increases with increasing acid concentration [14]. The change in the Si/Al molar ratio in samples subjected to heat treatment at different temperatures and then treated with hydrochloric acid solutions of various concentrations is shown in Fig. 8.

As can be seen from Fig. 8, pre-heat treatment significantly reduces the degree of dealumination, especially for samples partially or completely amorphized by high-temperature calcination. Perhaps these results are not of practical importance, since at an annealing temperature of 600 °C and above, the corresponding samples lose their adsorption properties (see Fig. 5), but the structure and properties of the- calcined and acid-treated samples require further study.

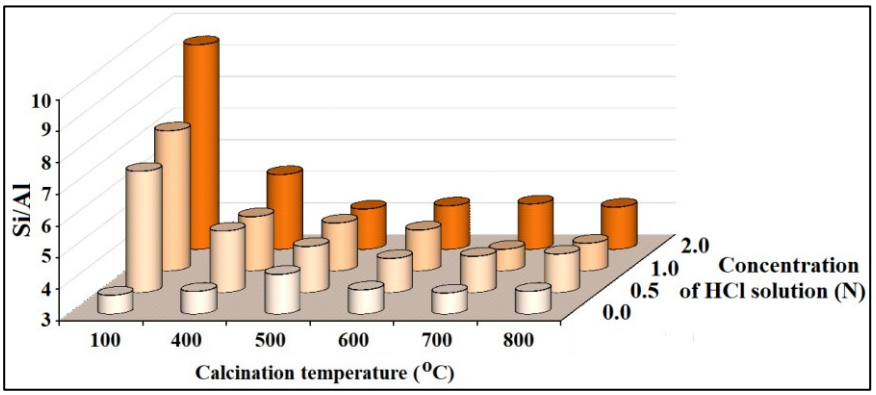

Fig. 8. The Si/Al molar ratio in samples calcined at different temperatures and treated with HCl solutions of various concentrations calculated from XRED spectra.

Conclusion

The effect of heat on the heulandite-containing tuff from the Tedzami-Dzegvi deposit leads to slight dealumination of the surface of the calcined (400-500 °C) samples, as well as to dehydration, amorphization of the crystal structure, and changes in the system of mesopores. Amorphization of the heulandite phase begins at temperatures above 200 °C, the transition to the heulandite B phase at ≈340 ºC is not fixed either on the TGA curve or by XRD patterns, but at high temperatures wairakite and/or another mineral of the 9.GB.05 group are formed; complete dehydration of the sample is achieved at ≈800 ºC. The BET surface area decreases monotonically from 12.8 to 6.5 m^2/g with an increase in the calcination temperature, but the average mesopore diameters calculated from the BET and BJH models change nonmonotonically without visible changes in the pore size distribution curves. It is also shown that heat treatment increases the acid resistance of heulandite by reducing the degree of dealumination after the sample is treated with hydrochloric acid solution.

The obtained data on the stability of the structure of Georgian natural heulandite should be taken into account both when determining its operating conditions and when using heat treatment as a tool to improve its properties.

Acknowledgments

This work was supported by Shota Rustaveli National Science Foundation of Georgia (SRNSFG) [grant number AR-22-610, Project Title “Production of paper with bactericidal and improved surface properties”].

References

1. G. W. Hardi, M. A. J. Maras, Y. R. R. Riva, and S. F. Rahman, "A review of natural zeolites and their applications: Environmental and industrial perspectives. International Journal of Applied Engineering Research," vol. 15(7), pp. 730-734, 2020.
2. Y. Li, and J. Yu, "Emerging applications of zeolites in catalysis, separation and host–guest assembly," Nature Reviews Materials, vol. 6, pp. 1156–1174, 2021.
3. B. Ma, and B. Lothenbach, "Synthesis, characterization, and thermodynamic study of selected K-based zeolites", Cement Concrete Res., vol. 148, # 106537, pp. 1-18, 2021.
4. A. Grela, J. Kuc, and T. Bajda, "A review of the application of zeolites and mesoporous silica materials in the removal of non-steroidal anti-flammatory drugs and antibiotics from water", Materials, vol. 14(17), # 4994, pp. 1-24, 2021.
5. M. Koizumi, "The differential thermal analysis curves and the dehydration curves of zeolites", Mineralogical J., vol. 1(1), pp. 36-47, 1953.
6. F. A. Mumpton, "Clinoptilolite redefined", Amer. Mineral., vol. 45, pp. 351-369, 1960.
7. F. Pechar, and D. Rykl, "Study of the thermal stability of the natural zeolite heulandite", Chem. Pap., vol 39(3), pp. 369-377, 1985.
8. V. Tsitsishvili, M. Panayotova, M. Miyamoto, N. Dolaberidze, N. Mirdzveli, M. Nijaradze, Z. Amiridze, N. Klarjeishvili, B. Khutsishvili, N. Dzhakipbekova, L. Harutyunyan, "Characterization of Georgian, Kazakh and Armenian natural heulandite-clinoptilolites", Bull. Georg. Natl Acad. Sci., vol. 16(4), pp. 115–122, 2022.
9. Ch. Baerlocher, L. B. McCusker, and D. H. Olson (eds.), "Atlas of zeolite framework types," Elsevier, Amsterdam, 2007.
10. G. V. Tsitsishvili, T. G. Andronikashvili, G. N. Kirov, and L. D. Filizova, "Natural zeolites," Ellis Horwood, Chichester (UK), 1992.
11. M. M. J. Treacy, and J. B. Higgins (eds.), "Collection of simulated XRD powder patterns for zeolites," Elsevier, Amsterdam, 2001.
12. L. Dang, S. Le, R. Lobo, and T. Pham, "Hydrothermal synthesis of alkali-free chabazite zeolites," J. Porous Mat., vol 27, pp. 1481-1489, 2020.
13. S. Yamaka, P. B. Malla, and S. Komarnani, "Water sorption and desorption isotherms of some naturally occurring zeolites," Zeolites, vol. 9(1), pp. 18-22, 1989.
14. V. Tsitsishvili, N. Dolaberidze, N. Mirdzveli, M. Nijaradze, N. Dzhakipbekova, L. Harutyunyan, Z. Amiridze, and B. Khutsishvili, "Acid treatment of Georgian, Kazakhstani and Armenian natural heulandite-clinoptilolites", 1st Int. Sci. Pract. Conf. "Sci.: Devel. Fact. Infl.", InterConf, vol. 138, pp. 363-370, 2022